RSC Advances

PAPER

View Article Online
View Journal | View Issue

Cite this: *RSC Adv.*, 2015, **5**, 79239

Combining amphiphilic chitosan and bioglass for mediating cellular osteogenic growth peptide gene†

Jie Luo,[ab] You Ling,[ab] Xian Li,[ab] Bo Yuan,[c] Feng Yu,[ab] Weihan Xie[ab] and Xiaofeng Chen*[abc]

Received 11th July 2015
Accepted 3rd September 2015

DOI: 10.1039/c5ra13628h

www.rsc.org/advances

The realization of gene therapy significantly depends on effective gene delivery vectors. Bioactive glasses (BG), as osteoinductive bone repair materials have been extensively applied clinically. Although there are numerous studies about the delivery of biomolecules by BG, to date, little study has been done to investigate the impact of BG as an enhancer for polymers/DNA complexes. In our study, we used an MBG with a suitable size to evaluate the influence of CS-PCL-mPEG/pOGP (containing the osteogenic growth peptide and green fluorescent protein fusion gene) on the gene transfection in different types of cell lines. MBG/CS-PCL-mPEG condense and dissociate the pOGP more effectively. These complexes, which are connected by the electrostatic effect, show lower and optimized zeta potential and size below 200 nm. Our study shows that MBG has good cellular biocompatibility and high cell uptake. MBG/CS-PCL-mPEG exhibits enhanced gene transfection efficiency despite the difference between the two cell lines. These results suggest that MBG has an enhanced impact on the polymer gene vectors. Therefore, this strategy may broaden the biomedical application of bioglass in the repair and reconstruction of bone and teeth.

1. Introduction

Gene therapy is considered to be a promising approach for the treatment of innate and acquired diseases.[1,2] The realization of gene therapy significantly depends on the effective gene delivery vectors.[3] Viral vectors, such as retrovirus, adenovirus and lentivirus, show high transfection efficiency but at the same time immunogenicity and potential infectivity for the practical applications.[4] Therefore, various types of non-viral vectors, such as synthetic polymers, lipids, and calcium phosphate nanoparticles, have attracted considerable attention since their emergence, due to their distinct advantages over viral counterparts that include ease of synthesis, low immunogenicity, and great safety measures.[5,6] However, the low transfection efficiency compared to viral systems is a large obstacle to their applications. Therefore, extensive efforts have been made to develop new composite materials for high efficiency gene transfection with low cytotoxicity.

With the rapid development of bone tissue engineering in recent years, osteoinductive bone repair materials have been extensively applied clinically.[7,8] Among these, bioceramic materials, such as hydroxyapatite, calcium phosphates, bioactive glasses (BG), and related composite materials, are used widely in bone tissue engineering.[9,10] BG was first developed by Hench and co-workers in 1969,[11] which took the form of blocks or crushed micron particles with specific compositions. BG shows excellent biocompatibility and biological mineralization due to the chemical reactions that occur on the material surface.[12] Ion dissolution products released from BG can result in an active apatite surface layer,[13,14] up-regulation of osteogenic gene expression,[15] stimulation of osteoblast proliferation and differentiation,[16,17] and increasing secretion of vascular endothelial growth factor (VEGF).[18–20] These typical characteristics and favorable responses of BG contribute to its bioactivity and promote rapid bone formation.

About a decade ago, a new type of BG, called mesoporous bioglass (MBG), was developed by Yan and coworkers,[21] through a combination of the sol–gel method and the supramolecular chemistry of surfactants. MBG possesses uniform and adequate mesoporosity, controllable nanopore size and pore volume, excellent cytocompatibility and apatite mineralization.[22] Based on favorable properties, MBG has attracted increasing attention. The important potential of MBG is that it can load and deliver biomolecules such as chemical drugs and siRNA.[23] The mesoporous structures, preparation methods, and even the

[a]*School of Materials Science and Engineering, South China University of Technology, Guangzhou, 510641, China. E-mail: chenxf@scut.edu.cn; Fax: +86-20-22236083*

[b]*National Engineering Research Center for Tissue Restoration and Reconstruction, South China University of Technology, Guangzhou, 510006, China*

[c]*Key Laboratory of Biomedical Materials and Engineering, Ministry of Education, Guangzhou, 510006, China*

† Electronic supplementary information (ESI) available: The characterization of CS-PCL-mPEG, the value of critical micelle concentration (CMC) and the recombinant plasmid pOGP. See DOI: 10.1039/c5ra13628h

dissolution of MBG are extremely important for influencing biomolecule delivery.[24] It has also been shown that the control of the particle size is a critical issue in achieving satisfactory transfection efficiency.[25] We recently reported[26] that MBG nanoparticles, which were about 200 nm in size, showed a potential to deliver the osteoactivin gene.

Although there are studies about the delivery of biomolecules by MBG, very few studies have been carried out to investigate the impact of MBG as an enhancer for polymers/DNA complexes. In our present study, on the one hand, the smaller size of MBG, which was about 140 nm, has been found to be suitable for gene transfection; on the other hand, the amphiphilic chitosan (CS), including PEG as a hydrophilic segment and polycaprolactone (PCL) as a hydrophobic one, has been investigated as a gene vector due to its self-assembly to form micelles in aqueous solutions.[27,28] The aim of our present study is to evaluate the influence of MBG for the gene transfection of CS-PCL-mPEG/pOGP complexes in different types of cell lines. Osteogenic growth peptide (OGP) was chosen as a model gene, which can induce differentiation of osteoblasts. The designed model gene has 4.7 kb, which is longer than siRNA or EGFP gene and more difficult to be delivered. The MBG/CS-PCL-mPEG/pOGP complexes were investigated in terms of zeta potential, particle size, pOGP binding ability, and *in vitro* pOGP release. The *in vitro* gene transfection efficiency of the complexes was monitored in two cell lines (HeLa and MG63).

2. Materials and methods

2.1 Materials

CS (deacetylation degree = 92.20, determined by element analysis and ^{1}H NMR spectra, molecular weight = ~100 kDa) was purchased from Golden Shell Biochemical Co. Ltd (Zhejiang, China). Tetraethyl orthosilicate (TEOS), triethyl phosphate (TEP), calcium nitrate tetrahydrate (CN), ethanol (EtOH), ethyl acetate (EA) and ammonium hydroxide (NH_4OH) were purchased from Guangzhou Chemical Reagent Factory. Pyridine, ε-caprolactone and mPEG were supplied by Sigma-Aldrich (St. Louis, MO, USA). DNase I and plasmid OGP were obtained from Thermo Fisher Scientific Inc. (Waltham, MA, USA). Gelred™ (10 000×) was purchased from Biotium Inc. (Hayward, CA, USA). Gel loading buffer (10×) was supplied by Takara Bio Inc. (Japan). Cell Counting Kit-8 was purchased from Dojindo Laboratories (Kumamoto, Japan). HeLa cell lines supplied by the Institute of Biochemistry and Cell Biology, SIBS, CAS (Shanghai, China) were cultured in Dulbecco's modified Eagle's medium (DMEM, GIBCO, Carlsbad, CA, USA) supplemented with 10% fetal bovine serum (FBS, Carlsbad, CA, USA). All the other chemicals and reagents were of analytical grade and used without further purification.

2.2 Construction of recombinant plasmid pOGP

A full-length OGP sequence was found in the universal GenBank database and was purchased from Thermo Company. The resulting products were digested with Xho I/Hind III and then cloned into the mammalian cell expression vector, pAc-EGFP-N1. Plasmids were verified by PCR, enzyme digestion and sequence analysis until the results showed that the gene sequence was correct. The recombinant plasmid (Fig. S1†) included OGP, GFP, and Kanamycin resistance gene. We named the recombinant plasmid as pOGP.

2.3 Formation of complexes

CS-PCL-mPEG was prepared based on the method available in the literature.[27] The novel MBG was synthesized based on our recent study.[29] CS-PCL-mPEG/pOGP and MBG/CS-PCL-mPEG/pOGP complexes were prepared as follows. CS-PCL-mPEG solutions were prepared by dissolving the polymers in 20 mM sodium acetate buffer (pH = 6.5) and then filtered through 0.2 μm cellulose acetate syringe filters (VWR International, IL, USA). The pOGP solutions were also prepared in 20 mM sodium acetate buffer (pH = 6.5). The CS-PCL-mPEG/pOGP complexes at various weight ratios were then formulated by mixing the CS-PCL-mPEG solution (*e.g.*, 2.5 mg mL^{-1}) with the pOGP solution (*e.g.*, 200 μg mL^{-1}) at a desired concentration. Finally, the MBG/CS-PCL-mPEG/pOGP complexes at various weight ratios were prepared by adding the MBG solutions directly to the CS-PCL-mPEG/pOGP mixture and mixing by pipetting. The complexes were incubated at room temperature for 40 min before further characterization.

In this study, the specific ratios were determined by following the rules if there were no special instructions in the corresponding section. On the one hand, CS-PCL-mPEG/pOGP had different weight ratios of 1, 5, 10, 20, and 50. On the other hand, for the MBG/CS-PCL-mPEG/pOGP complexes, the weight ratio of CS-PCL-mPEG/pOGP was set to 20, which was the optimized weight ratio for all gene transfection studies (data not shown). Therefore, the weight ratio of MBG/pOGP was in terms of that of MBG/CS-PCL-mPEG. In the whole experiment, the weight ratios of MBG/CS-PCL-mPEG were 1 : 20, 2 : 20, 4 : 20, 6 : 20, and 8 : 20.

2.4 Morphology of complexes

The morphology of CS-PCL-mPEG and MBG/CS-PCL-mPEG was examined *via* scanning electron microscopy (SEM, Merlin, Zeiss, Germany) at an accelerating voltage of 5.00 kV. The sample was coated with gold for 180 s under a gas pressure of 50 mTorr. The particle size and mesoporous structure of the nanoparticles were also observed by high-resolution transmission electron microscopy (TEM) using a JEM-2100HR apparatus (JEOL, Japan).

2.5 Gel retardation assay

The formation of complexes was assessed by agarose gel electrophoresis. To prepare complexes (100 μL total volume) at different weight ratios, 10 μg of pOGP was mixed with different concentrations of CS-PCL-mPEG and MBG/CS-PCL-mPEG solutions. The complexes were incubated at room temperature for 30 min. Subsequently, 2 μL of gel loading buffer (10×) was added to the complexes (10 μL), and the mixture was loaded on a 1% (w/v) agarose gel containing gel red (10 000×).

The electrophoresis was performed at 80 V for 60 min in 1 × TAE (Bio-Rad, CA, USA) buffer. The pOGP migration patterns were visualized on a VDS thermal imaging system (Bio-Rad, CA, USA). According to the literature,[8] each complex (300 μL) at different weight ratios, which contained 30 μg pOGP, was centrifuged at 20 000*g* for 20 min, and the pOGP concentration in the supernatant was measured by Nanodrop 3300 (Thermo, Waltham, MA, USA). The pOGP encapsulation efficacy (%) was calculated using the following equation:

$$\text{Encapsulation efficacy (\%)} = [(\text{initial pOGP concentration} - \text{supernatant pOGP concentration}) / \text{initial pOGP concentration}] \times 100\%.$$

2.6 DNase I protection

The resistance of the MBG/CS-PCL-mPEG/pOGP complexes to pOGP hydrolysis by endonucleases was measured by DNase I protection assay. The complexes containing 2 μg of pOGP at certain weight ratios were incubated with 0.5 units of DNase I in a reaction buffer solution (10 mM Tris–HCl, 2.5 mM $MgCl_2$, and 0.1 mM $CaCl_2$, pH 7.5) at 37 °C for 30 min. Subsequently, 0.5 μL of 50 mM EDTA was added to inactivate DNase I and the mixture was incubated at 65 °C for 10 min. An analysis of pOGP degradation was performed by gel electrophoresis.

2.7 Zeta potential and particle size

Two complexes were prepared at various weight ratios in 20 mM sodium acetate buffer (pH = 6.5) with a pOGP concentration of 20 μg mL^{-1}. Particle sizes and zeta potentials were measured using a Zetasizer Nano-ZS (Malvern Instruments, Malvern, UK) instrument, which was equipped with a nominal 5 mW He–Ne laser operating at 633 nm and at a constant scattering angle of 90°.

2.8 *In vitro* release

Two complexes, containing 25 μg of pOGP, were dispersed in 500 μL of PBS (pH = 7.4). The suspension of the complexes was incubated at 37 °C under agitation. At predetermined intervals, the suspension was centrifuged at 30 000*g*, 4 °C for 20 min. The amount of pOGP released in the supernatant was analyzed by Nanodrop 3300 (Thermo, Waltham, MA, USA).

2.9 Cell viability

The *in vitro* cytotoxicity of THE MBG/CS-PCL-mPEG/pOGP complexes was evaluated by CCK-8 assay. HeLa cells, which were cultured in 100 μL of H-DMEM containing 10% FBS at 37 °C in 5% CO_2, were seeded at a density of 5×10^3 cells per well in 96-well plates for 24 h. MG63 cells were cultured in L-DMEM containing 10% FBS. Subsequently, the complexes at various weight ratios were added to the cells. At predetermined intervals, 10 μL of CCK-8 was added to each well and incubated for 1 h. The absorbance of each sample was measured at 450 nm using a microplate reader (Thermo 3001, USA). The cells untreated with complexes in the cultures were used as the control. Cell viability was calculated by the following equation:

$$\text{Cell viability (\%)} = [(\text{experimental group absorbance} - \text{background absorbance}) / (\text{control absorbance} - \text{background absorbance})] \times 100\%.$$

2.10 Cellular uptake of complexes

To evaluate cellular uptake, CS-PCL-mPEG and MBG/CS-PCL-mPEG were covalently labeled with fluorescein 5-isothiocyanate (FITC). HeLa and MG63 cells were seeded in 24-well plates at 5×10^4 cells per well 20 h prior to the assay. The cells were then incubated with the FITC-labeled complexes containing 5 μg of pOGP per well. After 4 h of incubation at 37 °C, the uptake process was terminated by discarding the culture media containing complexes and rinsing the cells three times with PBS. The cells were then collected by trypsinization and analyzed *via* flow cytometry (FACSAriaTM, BD, USA) to measure the percentage of FITC-positive cells.

2.11 *In vitro* gene transfection

The gene transfection of complexes was investigated in two cell lines. The cells were seeded in 24-well plates at 5×10^4 cells per well and cultured in 1 mL of DMEM supplemented with 10% FBS for 20 h prior to the assay. The medium was then replaced by the complexes solution containing 5 μg pOGP per well. After 4 h of incubation, the medium was exchanged with a fresh medium (DMEM with 10% FBS) for another 24 h. Naked pOGP was used as the control. The percentage of transfected cells was analyzed by flow cytometry. The transfected cells were also visualized and photographed *via* confocal laser scanning microscopy (TCS SP8, Leica, Germany).

2.12 Ion release

To elucidate the benefits of adding MBG in the delivery system of CS-PCL-mPEG/pOGP complexes, ion released from MBG was investigated. Three types of BG (irregular shape BG,[9] big sphere BG[10] and MBG) were chosen and the composition of these different types was designed in terms of the ratio of 58S (60 mol% SiO_2 : 36 mol% CaO : 4 mol% P_2O_5). The complexes were set at a weight ratio of 6 : 20 and each specimen (30 mg) was immersed in 30 mL DMEM solution for different times at 37 °C. The suspension was centrifuged and the ionic concentrations of Si, Ca and P were analyzed by inductively coupled plasma atomic emission spectrometry (ICP-AES, Perkin-Elmer Optima 5300DV, USA). Finally, the gene delivery efficiency of these complexes was investigated by flow cytometry.

2.13 Statistical analysis

All the experiments were repeated in triplicate unless otherwise noted. Statistical analysis was performed using a *t*-test. The differences were judged to be significant at $p < 0.05$.

3. Results

3.1 Morphology characterization

CS-PCL-mPEG was prepared (Fig. S2 and S3†) above the critical micelle concentration (CMC) (Tables S1 and S2†). The size of CS-PCL-mPEG and MBG/CS-PCL-mPEG was determined by Zetasizer Nano-ZS and SEM (Fig. 1). As shown by SEM, MBG exhibits a regularly spherical morphology with a corrosive pore; however, the surface of MBG/CS-PCL-mPEG becomes slightly smooth. From the Zetasizer Nano-ZS results, the average size of MBG and MBG/CS-PCL-mPEG is determined to be around 142.8 nm and 155.4 nm, respectively. Furthermore, the low average size value of the nanoparticles endows it with the advantage of endocytosis into cells.[30] As revealed by TEM (Fig. 2), the nanoparticles that were synthesized by the sacrificial liquid template method have a sea hedgehog-like morphology. Apparently, this morphology has an abundance of internal nanoporous structures.

3.2 Agarose gel electrophoresis

The binding abilities of complexes were monitored by agarose gel electrophoresis using naked pOGP as the control. The spontaneous association of DNA with gene vectors and subsequent DNA condensation in aqueous media is a result of the strong electrostatic interactions. Therefore, the use of MBG is likely to influence their association.[31]

Fig. 3 displays the electrophoretic mobility of pOGP in the complexes composed of CS-PCL-mPEG alone or CS-PCL-mPEG and MBG. From Fig. 3A, the presence of partially dissociated pOGP bands indicates the formation of physically unstable complexes at a weight ratio of 1. With a weight ratio above 5, the migration of pOGP is absolutely retarded for the CS-PCL-mPEG/pOGP complexes. In addition, the pOGP binding capacity is preserved despite the modification of CS. As illustrated in Fig. 3B, the weight ratio 20 of CS-PCL-mPEG/pOGP is regarded as the most optimum condition according to the aforementioned experiment. pOGP is absolutely retarded regardless of the MBG/CS-PCL-mPEG weight ratio, which is consistent with the data of encapsulation efficacy (Table 1). In other words, MBG, as a negative segment, has not changed the whole MBG/CS-PCL-mPEG charge from positive to negative.

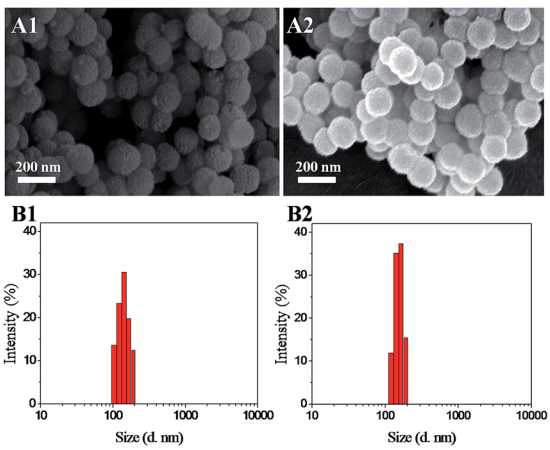

Fig. 1 The SEM images (A) and size distribution (B) of the complexes. A1 and B1 are MBG nanoparticles and A2 and B2 are MBG/CS-PCL-mPEG nanoparticles. The results are expressed as the mean ± SD ($n = 5$).

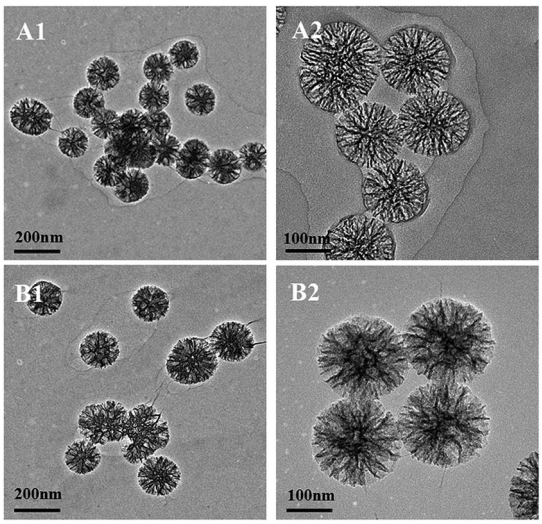

Fig. 2 The TEM images of MBG (A1 and A2) and MBG/CS-PCL-mPEG (B1 and B2).

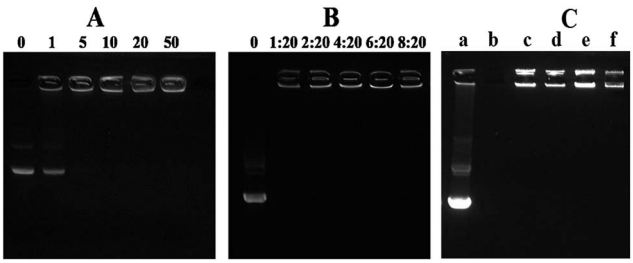

Fig. 3 Agarose gel electrophoresis of pOGP complexed with CS-PCL-mPEG (A) and MBG/CS-PCL-mPEG (B) at different weight ratios using 1% agarose gel. Based on the optimized weight ratio of 20 in CS-PCL-mPEG/pOGP, weight ratios of MBG/CS-PCL-mPEG were set to 1 : 20, 2 : 20, 4 : 20, 6 : 20, and 8 : 20. (C) DNase I protection assay. (a) pOGP, (b) pOGP + DNase I, (c) MBG/CS-PCL-mPEG/pOGP (1 : 20), (d) MBG/CS-PCL-mPEG/pOGP (1 : 20) + DNase I, (e) MBG/CS-PCL-mPEG/pOGP (8 : 20), and (f) MBG/CS-PCL-mPEG/pOGP (8 : 20) + DNase I.

Table 1 The encapsulation efficacy of pOGP in MBG/CS-PCL-mPEG at different weight ratios

MBG/CS-*g*-PCL-*b*-mPEG	Encapsulation efficacy (%)
1 : 20	94.1 ± 2.2
2 : 20	92.7 ± 3.7
4 : 20	91.4 ± 2.9
6 : 20	92.1 ± 3.5
8 : 20	90.2 ± 2.4

3.3 Protection of pOGP against nucleases

The structural integrity of the therapeutic gene is a prerequisite to ensure its desired function *in vitro* as well as *in vivo*.

Therefore, an efficient gene vector must confer adequate protection to pOGP against nuclease degradation. The pOGP protection capacity of the complexes was evaluated by agarose gel electrophoresis using DNase I as a model enzyme. As demonstrated in Fig. 3C, MBG/CS-PCL-mPEG complexes have the complete ability to protect pOGP from DNase I degradation at different weight ratios. The data for 2 : 20, 4 : 20, and 6 : 20 is not shown due to the same outcome compared to the data of 1 : 20 and 8 : 20.

3.4 Zeta potential and particle size

Particle size and zeta potential play an important role in the cellular uptake rate of complexes. To monitor the effect of the addition of MBG on CS-PCL-mPEG/pOGP complexes, two types of complexes (CS-PCL-mPEG/pOGP and MBG/CS-PCL-mPEG/pOGP) were measured by Zetasizer Nano-ZS at different weight ratios.

As depicted in Fig. 4A, CS-PCL-mPEG/pOGP complexes have negative potentials at the weight ratio of 1, indicating that the amount of complexes is inadequate to completely condense pOGP. As the weight ratio increases, the zeta potentials of complexes change from negative to positive, and they reach a plateau at a weight ratio of 20. Compared to the CS-PCL-mPEG/pOGP complexes at the optimized weight ratio of 20, the MBG/CS-PCL-mPEG/pOGP complexes show lower zeta potentials at different weight ratios, which results from electrostatic effects of composite nanoparticles.[32–34] With increasing MBG content, the charge decreases. It can be noted that charge has not changed to negative and is higher than 7 mV.

The particle size (Fig. 4B) of CS-PCL-mPEG/pOGP complexes tends to decrease rapidly with increasing weight ratio, indicating the formation of condensed complexes because of the presence of a higher density of available protonated amines of CS. Among them, the particle size of the CS-PCL-mPEG/pOGP complexes was around 171.2 nm at a weight ratio of 20. We suppose that amphiphilic CS-PCL-mPEG/pOGP complexes tend to form small nanoparticles, as a result of the more compressed nanoparticles by hydrophobic segments in an aqueous solution.[30] Furthermore, the average particle size of MBG/CS-PCL-mPEG/pOGP remained fairly constant at about 176.3 nm when the MBG was added. To some extent, this may indicate that MBG is regarded as a core and the whole complexes size could not be changed.[33]

The influence of adding MBG is significant for zeta potential, but it is little for particle size.

3.5 *In vitro* release of pOGP

To avoid lysosomal entrapment, complexes have to move towards the cell nucleus and then unload/release the DNA

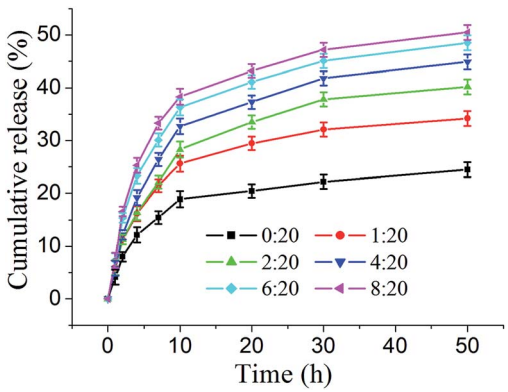

Fig. 5 Cumulative pOGP release profiles of CS-PCL-mPEG/pOGP at an optimized weight ratio of 20 and MBG/CS-PCL-mPEG/pOGP at weight ratios of 1 : 20, 2 : 20, 4 : 20, 6 : 20, and 8 : 20.

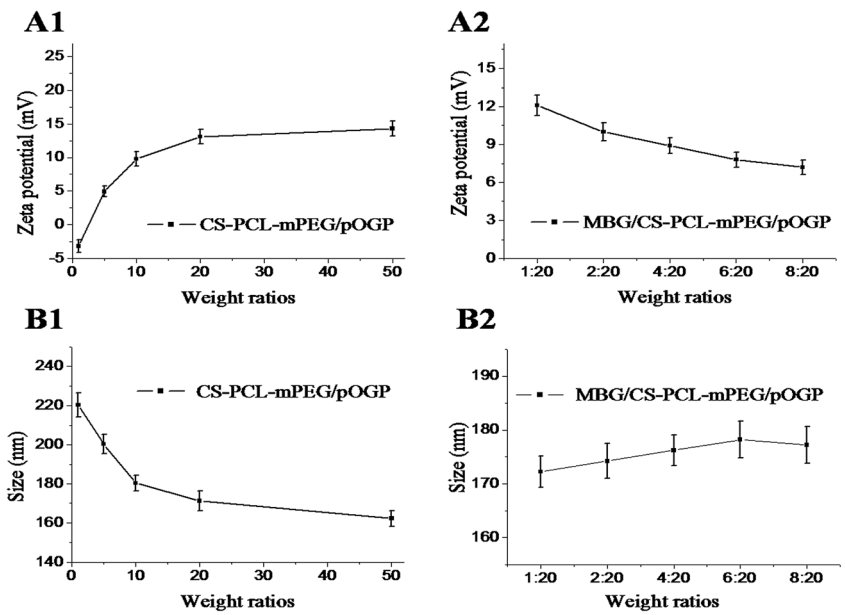

Fig. 4 Zeta potential (A) and average particle size (B) of the two complexes. All the measurements were performed after the complexes were incubated for 30 min at room temperature.

inside for transcription.[35] The very strong interaction between the delivery vectors and pOGP will impose difficulty on the dissociation of condensed pOGP and thereby decrease the gene transfection efficiency. Thus, the accumulated release profile of the condensed pOGP plays a significant role in modulating the overall gene expression.

The accumulated release profile of CS-PCL-mPEG/pOGP at the weight ratio of 20 in pH 7.4 PBS is shown in Fig. 5. After 50 h of incubation, the cumulative release percentage increases to 24.5%. However, MBG/CS-PCL-mPEG/pOGP at different weight ratios shows a higher release rate and increases to 34.2%, 40.2%, 44.9%, 48.5%, and 50.5%. These results are in complete agreement with the zeta potential and agarose gel electrophoresis data. The zeta potential decreased as MBG was added to the CS-PCL-mPEG/pOGP system, which has an important effect on the association and dissociation of pOGP. On the one hand, the decreasing positive charge of MBG/CS-PCL-mPEG has the absolute ability to condense pOGP in spite of adding MBG. On the other hand, the lower charge allows the easy escape of pOGP from the complexes as compared to the pure CS-PCL-mPEG/pOGP.

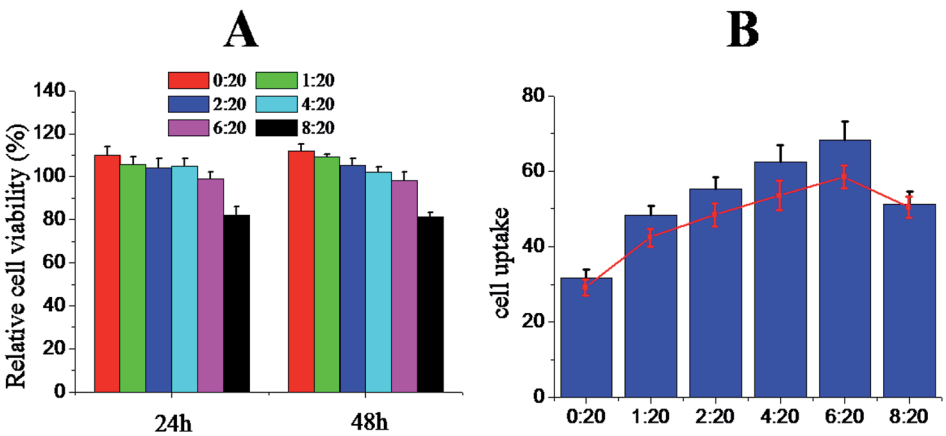

Fig. 6 (A) *In vitro* cytotoxicity of MBG/CS-PCL-mPEG/pOGP complexes in HeLa cells. (B) Cellular uptake of MBG/CS-PCL-mPEG/pOGP complexes in HeLa cells (blue bar) and MG63 (red line) following incubation at 37 °C for 4 h. The results are expressed as the mean ± SD ($n = 4$).

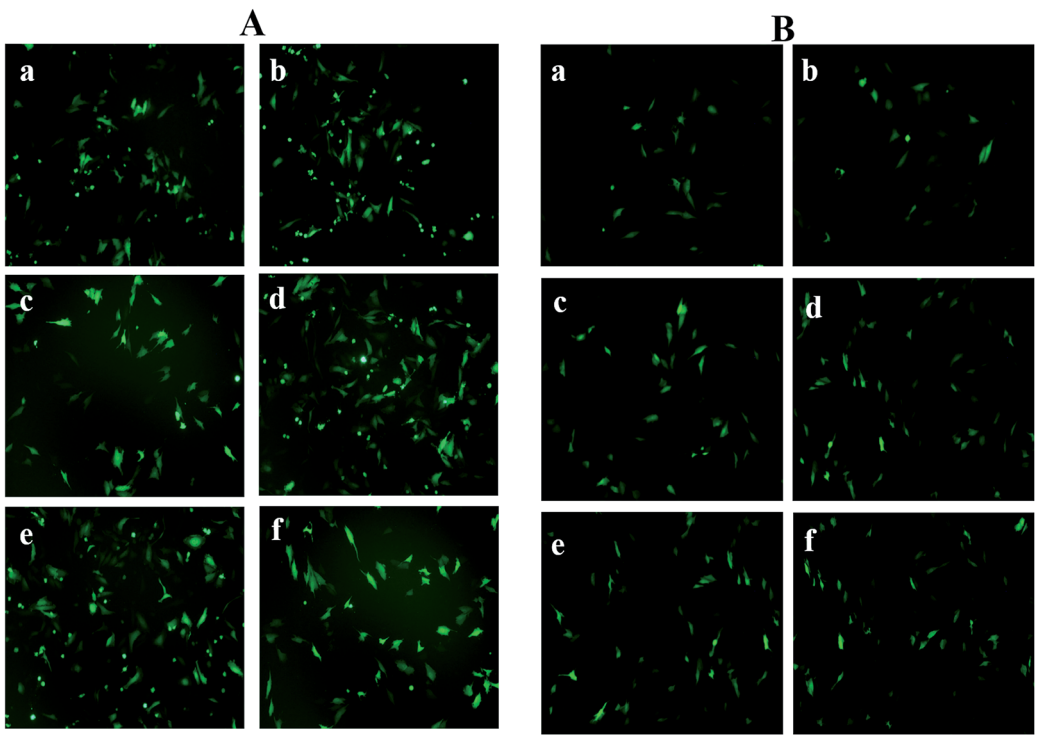

Fig. 7 Fluorescence images of HeLa (A) and MG63 (B) cells transfected with the MBG/CS-PCL-mPEG/pOGP complexes at different weight ratios of 0 : 20 (a), 1 : 20 (b), 2 : 20 (c), 4 : 20 (d), 6 : 20 (e), and 8 : 20 (f). Bar = 100 μm.

3.6 Cell viability

The cytotoxicity of complexes is regarded as a limiting factor for their *in vivo* applications. To investigate the influence of the presence of MBG in complexes in HeLa cells, the cell viability was determined by the CCK8 assay. The MG63 cells were also analyzed using this assay, but no cytotoxicity was found within the tested conditions (data not shown). The MBG/CS-PCL-PEG/pOGP ratios used in these assays were chosen according to their transfection efficiency. As shown in Fig. 6A, compared to the control, there is no significant change in the cells treated with MBG/CS-PCL-mPEG/pOGP complexes at the weight ratios of 1 : 20, 2 : 20, 4 : 20, and 6 : 20. However, the concentration of MBG at 8 : 20 leads to cell damage, and the cell viability was 81% when the HeLa cells were cultured at 48 h.

3.7 Cellular uptake

To properly track the cellular uptake process, CS-PCL-mPEG and MBG/CS-PCL-mPEG were covalently conjugated with FITC in two cells. As depicted in Fig. 6B, only a mean 31.8% FITC-positive HeLa cells are mediated by CS-PCL-mPEG/pOGP complexes at different weight ratios, whereas the uptake percentages are improved by 1.52–2.14 fold for the MBG/CS-PCL-mPEG/pOGP complexes. With increasing amount of MBG, the complexes at different weight ratios reach to 48.3%, 55.2%, 62.4%, 68.2%, and 51.3%. The results are consistent

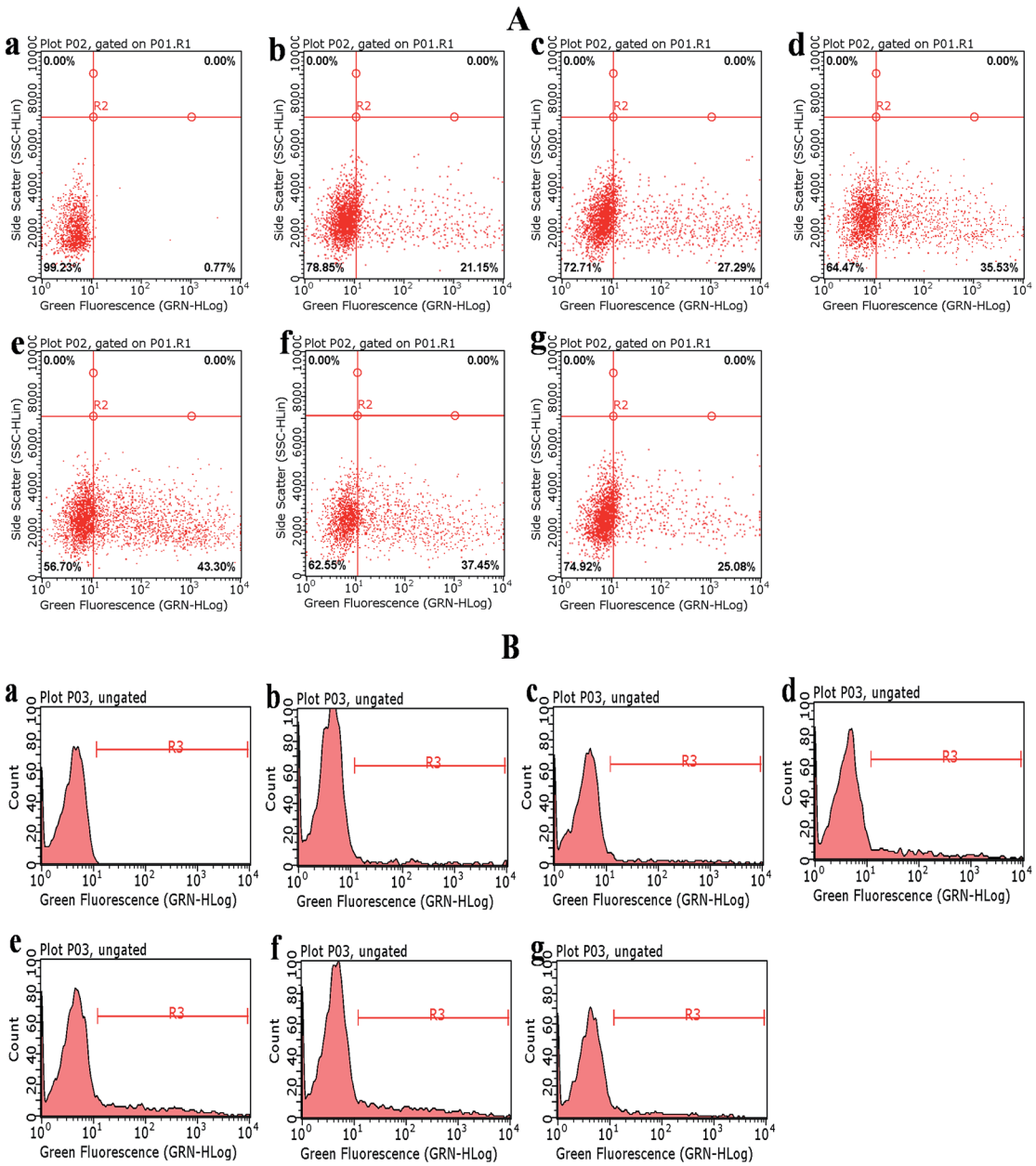

Fig. 8 Transfection efficiency of MBG/CS-PCL-mPEG complexed with pOGP as a reporter gene was determined by flow cytometry in HeLa (A) and MG63 (B) cells. (a) naked pOGP, (b) 0 : 20, (c) 1 : 20, (d) 2 : 20, (e) 4 : 20, (f) 6 : 20, and (g) 8 : 20.

with zeta potential data. Due to the negative potential of the cell membranes, the lower positive charge of complexes, which were attributed to the electrostatic self-assembly effects, is more suitable for entry to the HeLa cells. However, the concentration of MBG at a weight ratio of 8 : 20 is so high that the cells are damaged and the quantity of cells absorbing the complexes decrease. Furthermore, the MG63 cells have a similar situation.

3.8 *In vitro* transfection

To investigate the influence of MBG on *in vitro* gene transfection ability, two types of complexes were investigated on HeLa and MG63 cells using pOGP. HeLa cells have been extensively used as a standard model to evaluate gene transfection efficiency of non-viral vectors. For pOGP, which is related to the osteogenic gene, the MG63 cells were applied as a model to explore the gene transfection efficiency. To determine the optimal weight ratio of CS-PCL-mPEG/pOGP complexes for transfection, weight ratios ranging from 1 to 50 were investigated for initial screening, and the optimized weight ratio of 20 was used for all the transfection studies (data not shown).

The transfection efficiency of the complexes was visualized by confocal laser scanning microscopy. As illustrated in Fig. 7, MBG/CS-PCL-mPEG nanoparticles at different weight ratios exhibit higher transfection efficiency compared to CS-PCL-mPEG regardless of the cell lines. The percentages of transfected cells were also quantitatively determined by flow cytometry. As shown in Fig. 8, CS-PCL-mPEG/pOGP at the optimized weight ratio of 20 in HeLa and MG63 cells shows only 21.15% and 15.41% of transfected cells, respectively. However, MBG/CS-PCL-mPEG/pOGP complexes at the weight ratio of 4 : 20 in HeLa cells are found to mediate the high level of gene expression with 43.30% of transfected cells detected, which is 2-times higher than the corresponding CS-PCL-mPEG/pOGP complexes.

For MG63 cells, the highest level of gene expression is 29.92% at the weight ratio of 6 : 20 of complexes. In these two cell lines, the overdose of complexes at the highest weight ratio of 8 : 20 will lead to a decrease in the transfection efficiency due to the cytotoxicity.

In summary, the overall change can be explained by the zeta potential measurement data despite the fluctuation in different cell lines. Owing to the decreasing charge of complexes, the condensed pOGP will be released easily in the cytoplasm and subsequently transferred to the nucleus.[36] However, at a higher ratio of MBG, the situation changes. There are two factors concluded to analyze this phenomenon. The dissociation of pOGP in the complexes is so premature that it will be degraded by the enzyme.[37] Furthermore, according to the cell viability data, the cells treated with the higher concentration of MBG are also damaged so that the transfection efficiency becomes lower.

3.9 Ion release

The amphiphilic chitosan provides the foundation of transfection efficiency, and the MBG as a enhancer also plays an important role. Based on our previous investigation,[26,38] we tried to elucidate the benefits of adding MBG in the CS-PCL-mPEG/pOGP complexes delivery system.

The transfection process is complicated. To be a gene carrier, MBG must possess numerous other properties such as good biocompatibility, highly sustained DNA loading ability, protection of DNA from degradation, entering into cells, escaping from lysosome, and excellent releasing efficiency of genes in

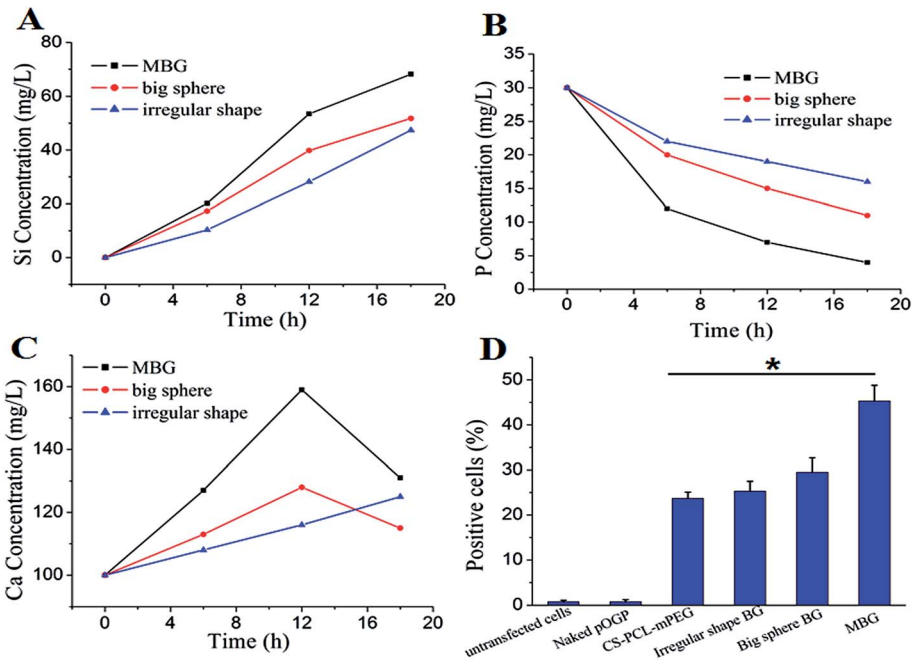

Fig. 9 Ion release profiles of different types of BG after soaking in DMEM for 18 h (A, B, and C). MBG (black line), big sphere (red line), and irregular shape (blue line), in which the designed composition is the same. Transfected cells with different types of complexes (D).

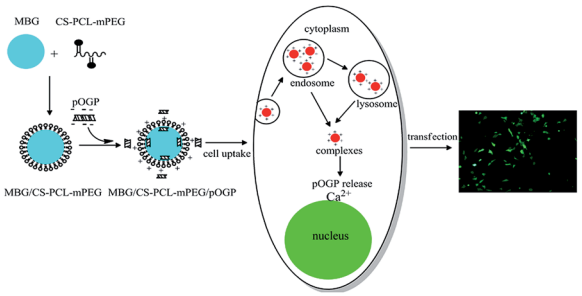

Fig. 10 Impact of MBG on the transfection.

cells. The genes can then be replicated, transcribed and finally translated into proteins.

Therefore, we try to propose the possible mechanisms for enhanced transfection from MBG. Hench supposed[39] the surface reactions release critical concentrations of soluble Si, Ca and P ions, which play a significant role in regulating the cell behavior. These ions give rise to both intracellular and extracellular responses at the interface of the glass with its cellular environment. Therefore, ion release is essential to acknowledge the influence on the gene transfection. As expected, due to the large pore size and high surface area, the MBG has the highest ion release rate of Ca^{2+} and highest consumption rate of PO_4^{3-} (Fig. 9A–C).

Based on our study,[26,38] the gene transfection efficiency has no difference between the transfected cells by the non-calcium bioglass and non-transfected cells (HeLa, MG63 and 293T). In addition, the amount of Ca^{2+} released is significantly different from the different types of BG. Therefore, we investigated the relationship of ion release and gene transfection using different types of BG. According to the literature,[40] an excess of soluble DNA in a supersaturated solution of calcium (Ca^{2+}) and phosphate (PO_4^{3-}) may prolong the period during which a precipitate forms. In other words, if the concentration is high enough, negative DNA could prevent precipitate formation partially to combine with Ca^{2+} by the electrostatic effects. Because the size of MBG used is lower than 190 nm, the complexes have higher cellular uptake (Fig. 6). Moreover, the complexes can confer adequate protection to pOGP against nuclease degradation (Fig. 3C). Therefore, in the cytoplasm, the greater combination of Ca^{2+}-pOGP plays an important role in the transfection efficiency, which is demonstrated by flow cytometry (Fig. 9D). The naked pOGP has no gene transfection efficiency due to cytoplasmic and nuclear degradation. Compared to the other types of BG, the MBG, which releases more Ca^{2+}, has the most capacity for combining the negative pOGP and subsequently realizes higher transfection efficiency. This is consistent with results reported by Choi *et al.* and Sandhu *et al.* (Fig. 10).[41,42]

4. Conclusions

This study evaluated the influence of MBG for the gene transfection of MBG/CS-mPEG-PCL in different types of cell lines. The recombinant plasmid pOGP containing OGP and GFP fusion gene was relatively large and very difficult to be delivered. It was illustrated that the incorporation of the MBG segment could condense pOGP more effectively. In addition, complex nanoparticles promoted the pOGP release rate due to the lower positive charge. Furthermore, MBG/CS-PCL-mPEG exhibited enhanced gene transfection efficiency than the pure polymers CS-PCL-mPEG. These findings highlighted MBG as an enhancer for chitosan vectors in gene therapy. The Ca^{2+} released from MBG plays a significant role in transfection. However, further exploration and research is needed for a detailed understanding of Ca^{2+} on the cell pathway.

Acknowledgements

This study was financially supported by the Specialized Research Fund for Doctoral Program of Higher Education of China (grant no. 20110172120002), the National Basic Research Program of China (973 Program) (grant no. 2011CB606204, 2012CB619100), the National Natural Science Foundation of China (grant no. 51172073, 51072055, 51202069, 51502094), the Key Project of the National Natural Science Foundation of China (grant no. 50830101), Project funded by the China Postdoctoral Science Foundation (2013M531853) and the Fundamental Research Funds for the Central University (grant no. 2014ZM0009, 2012ZP0001, 2013ZM0043, 2013ZB0005).

References

1 M. D. Buschmann, A. Merzouki, M. Lavertu, M. Thibault, M. Jean and V. Darras, *Adv. Drug Delivery Rev.*, 2013, **65**, 1234–1270.
2 L. Casettari, D. Vllasaliu, J. K. W. Lam, M. Soliman and L. Illum, *Biomaterials*, 2012, **33**, 7565–7583.
3 J. M. Dang and K. W. Leong, *Adv. Drug Delivery Rev.*, 2006, **58**, 487–499.
4 J. Suh, D. Wirtz and J. Hanes, *Proc. Natl. Acad. Sci. U. S. A.*, 2003, **100**, 3878–3882.
5 H. Yin, R. L. Kanasty, A. A. Eltoukhy, A. J. Vegas, J. R. Dorkin and D. G. Anderson, *Nat. Rev. Genet.*, 2014, **15**, 541–555.
6 W. Jun, D. Yamanouchi, L. Bo and C. Chih-Chang, *J. Mater. Chem.*, 2012, **22**, 18983–18991.
7 A. Oryan, S. Alidadi, A. Moshiri and A. Bigham-Sadegh, *BioFactors*, 2014, **40**, 459–481.
8 L. Brannon-Peppas, B. Ghosn, K. Roy and K. Cornetta, *Pharm. Res.*, 2007, **24**, 618–627.
9 R. Li, A. E. Clark and L. L. Hench, *J. Appl. Biomater.*, 1991, **2**, 231–239.
10 Q. Hu, X. Chen, N. Zhao and Y. Li, *Mater. Lett.*, 2013, **106**, 452–455.
11 L. L. Hench, R. J. Splinter, W. Allen and T. Greenlee, *J. Biomed. Mater. Res.*, 1971, **5**, 117–141.
12 L. L. Hench, *Am. Ceram. Soc. Bull.*, 1998, **77**, 67–74.
13 I. Christodoulou, L. D. Buttery, P. Saravanapavan, G. Tai, L. L. Hench and J. M. Polak, *J. Biomed. Mater. Res., Part B*, 2005, **74**, 529–537.
14 L. L. Hench, I. D. Xynos and J. M. Polak, *J. Biomater. Sci., Polym. Ed.*, 2004, **15**, 543–562.

15 I. D. Xynos, A. J. Edgar, L. D. Buttery, L. L. Hench and J. M. Polak, *Biochem. Biophys. Res. Commun.*, 2000, **276**, 461–465.
16 M.-A. Milona, J. E. Gough and A. J. Edgar, *BMC Genomics*, 2003, **4**, 43.
17 G. Jell and M. M. Stevens, *J. Mater. Sci.: Mater. Med.*, 2006, **17**, 997–1002.
18 A. A. Gorustovich, J. A. Roether and A. R. Boccaccini, *Tissue Eng., Part B*, 2009, **16**, 199–207.
19 A. Hoppe and A. Boccaccini, *Biomedical Foams for Tissue Engineering Applications*, Woodhead Publishing, 2014, pp. 191–212.
20 R. M. Day, *Tissue Eng.*, 2005, **11**, 768–777.
21 X. Yan, C. Yu, X. Zhou, J. Tang and D. Zhao, *Angew. Chem.*, 2004, **43**, 5980–5984.
22 M. S. Kang, J.-H. Kim, R. K. Singh, J.-H. Jang and H.-W. Kim, *Acta Biomater.*, 2015, **16**, 103–116.
23 A. El-Fiqi, T.-H. Kim, M. Kim, M. Eltohamy, J.-E. Won, E.-J. Lee and H.-W. Kim, *Nanoscale*, 2012, **4**, 7475–7488.
24 K. D. Patel, A. El-Fiqi, H.-Y. Lee, R. K. Singh, D.-A. Kim, H.-H. Lee and H.-W. Kim, *J. Mater. Chem.*, 2012, **22**, 24945–24956.
25 P. Lehn, S. Fabrega, N. Oudrhiri and J. Navarro, *Adv. Drug Delivery Rev.*, 1998, **30**, 5–11.
26 X. Li, X. Chen, G. Miao, H. Liu, C. Mao, G. Yuan, Q. Liang, X. Shen, C. Ning and X. Fu, *J. Mater. Chem. B*, 2014, **2**, 7045–7054.
27 L. Liu, X. Xu, S. Guo and W. Han, *Carbohydr. Polym.*, 2009, **75**, 401–407.
28 Y. Lu, L. Liu and S. Guo, *Biopolymers*, 2007, **86**, 403–408.
29 Q. Liang, Q. Hu, G. Miao, B. Yuan and X. Chen, *Mater. Lett.*, 2015, **148**, 45–49.
30 H. Tian, W. Xiong, J. Wei, Y. Wang, X. Chen, X. Jing and Q. Zhu, *Biomaterials*, 2007, **28**, 2899–2907.
31 S. Katayose and K. Kataoka, *J. Pharm. Sci.*, 1998, **87**, 160–163.
32 K. Kurita, H. Ikeda, Y. Yoshida, M. Shimojoh and M. Harata, *Biomacromolecules*, 2002, **3**, 1–4.
33 Y.-Q. Ye, F.-L. Yang, F.-Q. Hu, Y.-Z. Du, H. Yuan and H.-Y. Yu, *Int. J. Pharm.*, 2008, **352**, 294–301.
34 X.-J. Zhang, W. Huang, S. Yang, L.-D. Sun, F.-Y. Zhang, Q.-X. Zhu, F.-R. Zhang, C. Zhang, W.-H. Du and X.-M. Pu, *Nat. Genet.*, 2009, **41**, 205–210.
35 D. V. Schaffer, N. A. Fidelman, N. Dan and D. A. Lauffenburger, *Biotechnol. Bioeng.*, 2000, **67**, 598–606.
36 F. Zhou, L. Yuan, D. Li, H. Huang, T. Sun and H. Chen, *Colloids Surf., B*, 2012, **90**, 97–101.
37 L. Wang, X. Li, L. Yuan, H. Wang, H. Chen and J. L. Brash, *J. Mater. Chem. B*, 2015, **3**, 498–504.
38 H. Liu, X. F. Chen, X. Li, Y. L. Li and Z. F. Lin, *J. Inorg. Mater.*, 2014, **29**, 1023–1028.
39 L. L. Hench and J. M. Polak, *Science*, 2002, **295**, 1014–1017.
40 M. Jordan, A. Schallhorn and F. M. Wurm, *Nucleic Acids Res.*, 1996, **24**, 596–601.
41 S. Choi, X. Yu, L. Jongpaiboonkit, S. J. Hollister and W. L. Murphy, *Sci. Rep.*, 2013, **3**, 1–8.
42 A. P. Sandhu, A. M. I. Lam, D. B. Fenske, L. R. Palmer, M. Johnston and P. R. Cullis, *Anal. Biochem.*, 2005, **341**, 156–164.